JOURNAL OF GEOPHYSICAL RESEARCH, VOL. 103, NO. A7, PAGES 14,567–14,574, JULY 1, 1998

Proton resonant firehose instability: Temperature anisotropy and fluctuating field constraints

S. Peter Gary, Hui Li, Sean O'Rourke, and Dan Winske

Los Alamos National Laboratory, Los Alamos, New Mexico

Abstract. The electromagnetic proton firehose instability may grow in a plasma if the proton velocity distribution is approximately bi-Maxwellian and $T_{\|p} > T_{\perp p}$, where the directional subscripts denote directions relative to the background magnetic field. Linear Vlasov dispersion theory in a homogeneous electron-proton plasma implies an instability threshold condition at constant maximum growth rate $1-T_{\perp p}/T_{\|p} = S_p/\beta_{\|p}{}^{\alpha_p}$ over $1 < \beta_{\|p} \leq 10$ where $\beta_{\|p} \equiv 8\pi n_p T_{\|p}/B_o^2$ and B_o is the background magnetic field. Here S_p and α_p are fitting parameters and $\alpha_p \simeq 0.7$. One- and two-dimensional initial value hybrid simulations of this growing mode are carried out under proton cyclotron resonant conditions in a homogeneous plasma on the initial domain $2 \lesssim \beta_{\|p} \leq 100$. The two-dimensional simulations show that enhanced fluctuations from this instability impose a bound on the proton temperature anisotropy of the form of the above equation with the fluid theory result $\alpha_p \simeq 1.0$. On this domain both one- and two-dimensional simulations yield a new form for the upper bound on the fluctuating field energy density from the proton resonant firehose instability $|\delta B|^2/B_o^2 = S_B + \alpha_B \ln(\beta_{\|p})$ where S_B and α_B are empirical parameters which are functions of the initial growth rate. This logarithmic behavior is qualitatively different from a fluid theory prediction and, like the anisotropy bound, should be subject to observational verification in any sufficiently homogeneous plasma in which the proton velocity distribution is approximately bi-Maxwellian.

1. Introduction

A plasma anisotropy often leads to the growth of one or more short-wavelength instabilities, implying the presence not only of enhanced field fluctuations but also of wave-particle interactions which reduce that anisotropy. If the enhanced fluctuations are sufficiently weak and sufficiently broadband, the plasma response can be described by quasi-linear theory, implying that the linear growth rate is reduced either to zero or to a relatively small value. Then, following the procedure outlined by *Manheimer and Boris* [1977], the instability threshold condition becomes the limiting value of the anisotropy. This constraint can be obtained from linear theory and therefore corresponds to a relationship among plasma parameters which is independent of the field fluctuation amplitudes. If such a relationship is verified through observations in space or laboratory plasmas, it then may be used to represent the consequences of a kinetic plasma process in large-scale fluid models of anisotropic plasmas.

Kennel and Petschek [1966] used such a model to successfully predict the maximum anisotropies of energetic electron and ion distributions observed in the magnetosphere. More recently, research has been directed toward the thermal proton temperature anisotropy $T_{\perp p} > T_{\|p}$ where the perpendicular and parallel symbols denote directions relative to the background magnetic field $\mathbf{B}_o$. A direct correspondence has been shown between an upper bound on this anisotropy observed in the terrestrial magnetosheath [*Anderson et al.*, 1994; *Fuselier et al.*, 1994] and an anisotropy constraint derived from both linear theory and hybrid simulations of the electromagnetic proton cyclotron anisotropy instability [*Gary et al.*, 1997; and references therein]. Similarly, the imposition of an upper bound on the hot proton temperature anisotropy by this same instability in the outer magnetosphere has been predicted by theory and simulations [*Gary et al.*, 1995] and has been observed [*Anderson et al.*, 1996]. This anisotropy bound has been applied to large-scale anisotropic fluid models of both the terrestrial magnetosheath [*Denton and Lyon*, 1996, and references therein] and the magnetotail [*Birn et al.*, 1995].

The research described here addresses the proton temperature anisotropy $T_{\|p} > T_{\perp p}$. If the hot proton velocity distribution in a plasma is approximately bi-Maxwellian and bears such an anisotropy, then the proton firehose instability (or, more concisely, the firehose) may arise [*Parker*, 1958; *Vedenov and Sagdeev*, 1958]. This growing mode has a real frequency ω_r which satisfies $\omega_r < \Omega_p$ where Ω_p is the proton cyclotron frequency and, as various other symbols used in this manuscript, is defined in the Appendix.

The assumption that the protons are nonresonant with the fluctuating fields of the firehose is sometimes made. As we shall show, this is not generally valid. However, if this assumption is used in linear fluid theory with the condition that the growth rate is zero, it yields the instability condition for the nonresonant firehose [*Parker*, 1958; *Yoon*, 1990]:

$$1 - \frac{T_{\perp p}}{T_{\|p}} = \frac{2}{\beta_{\|p}} \qquad (1)$$

On the other hand, if one assumes only that the plasma is

Paper number 98JA01174.
0148-0227/98/98JA-01174$09.00

collisionless, then the Vlasov equation provides a more complete, more accurate description of the firehose. Section 2 addresses linear Vlasov solutions and discusses the parameter regimes in which the instability is resonant and nonresonant. Under resonant conditions the linear threshold condition for a fixed value of the dimensionless maximum growth rate γ_m/Ω_p of the proton firehose instability in an electron-proton plasma can be written for $\gamma_m/\Omega_p \leq 0.10$ as

$$1 - \frac{T_{\perp p}}{T_{\|p}} = \frac{S_p}{\beta_{\|p}{}^{\alpha_p}} \qquad (2)$$

over $1 \lesssim \beta_{\|p} \leq 10$. Here S_p and α_p are fitting parameters; the former is a dimensionless number of order unity determined by the choice of maximum growth rate, but $\alpha_p \simeq 0.7$, relatively independent of γ_m/Ω_p.

To understand the full consequences of instability growth, it is necessary to use nonlinear methods of study. For the proton resonant firehose instability, hybrid computer simulations [*Winske and Omidi*, 1993] are a highly appropriate tool. In a hybrid simulation the ions are represented as superparticles, but the electrons are given a simplified fluid representation. For the simulations described here the electrons are modeled as a massless fluid, so that the code provides a good description of the plasma physics corresponding to fluctuations below the proton cyclotron frequency.

Quest and Shapiro [1996] reported results from one-dimensional hybrid simulations of the proton firehose instability under the initial condition $T_{\perp p} = 0$. They found that as in simulations of other electromagnetic anisotropy instabilities, field fluctuations grow rapidly during an initial growth phase; at the same time the proton anisotropy is rapidly reduced. There follows a second stage of slower evolution during which the fluctuating field energy spectrum exhibits a cascade to longer wavelengths and the proton anisotropy reduction continues, although at a much slower rate.

Section 3 describes results from our one-dimensional hybrid simulations, and section 4 addresses conclusions from two-dimensional hybrid simulations. The former computations show many of the same characteristics as those of *Quest and Shapiro* [1996]. In addition, our results show that on the domain $2 \leq \beta_{\|p} \leq 100$ (2) with $\alpha_p \simeq 0.75$ represents a constraint on the proton temperature anisotropy imposed by enhanced field fluctuations from the proton firehose instability. These simulations also yield an empirical scaling relation for the maximum value of these fluctuations as

$$\frac{|\delta B|^2}{B_o^2} \equiv \frac{\sum_{\mathbf{k}} |\delta B_k|^2}{B_o^2} = S_B + \alpha_B \ln(\beta_{\|p}) \qquad (3)$$

where S_B and α_B are empirical parameters which depend upon the choice of maximum growth rate. Our two-dimensional simulations yield more stringent constraints on both the proton temperature anisotropy and the fluctuating fields; that is, S_p and α_B are uniformly smaller and $\alpha_p \simeq 2.0$ for the ensemble of two-dimensional simulations. All of our simulations yield much weaker scalings for the fluctuating magnetic field energy density than the fluid theory prediction of *Quest and Shapiro* [1996]:

$$\frac{|\delta B|^2}{B_o^2} = \frac{\beta_{\|p} - 2}{4} \qquad (4)$$

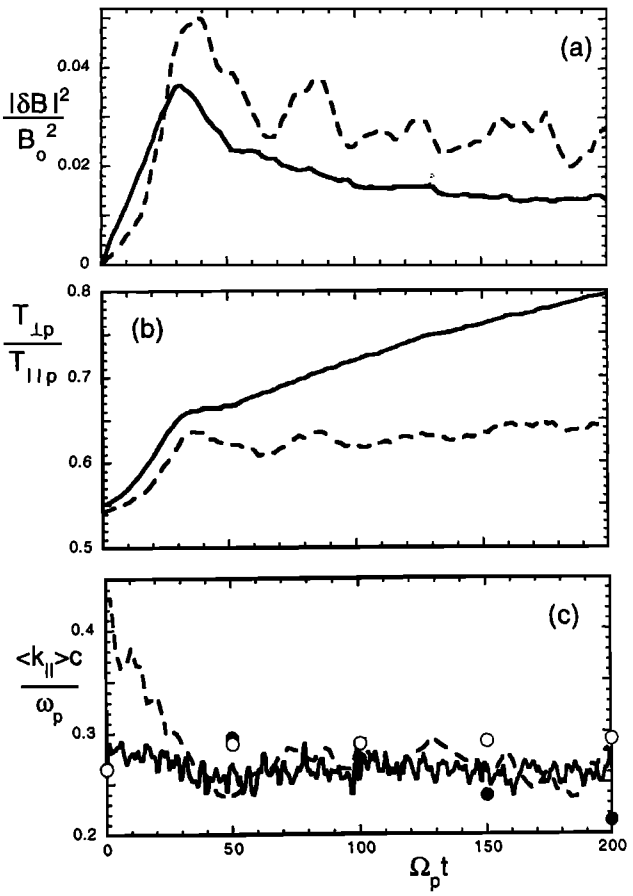

Figure 1. Results as functions of time from one-dimensional (dashed lines) and two-dimensional (solid lines) simulations using the same initial physical parameters, $\beta_{\|p} = 5.00$ and $T_{\perp p}/T_{\|p} = 0.55$, corresponding to $\gamma_m/\Omega_p = 0.10$ and $L\omega_p/c = 94.0$: (a) Fluctuating magnetic field energy density, (b) proton temperature anisotropy, and (c) average wavevector component parallel to B_o. The one-dimensional run utilized 64 cells with 256 particles per cell, whereas the two-dimensional run used a 64×64 grid with 64 particles per cell.

We attribute this difference to the resonant character of our simulations; at a given fluctuation amplitude, resonant wave-particle interactions are much more effective than nonresonant interactions and require much weaker amplitudes to scatter particles. Section 5 summarizes our conclusions.

Figure 1 compares results from two runs with the same initial physical conditions to illustrate some general differences between one- and two-dimensional simulations of the resonant firehose. Although the total fluctuating field energy density is relatively weaker in the two-dimensional case both at saturation and at subsequent times, wave-particle scattering, indicated by the rate of proton anisotropy reduction, is more efficient in the two-dimensional run. We interpret this difference as being due to the greater number of degrees of freedom in the two-dimensional case; as *Karimabadi et al.* [1992] have shown, the presence of electromagnetic waves propagating at oblique angles to $\mathbf{B}_o$ significantly enhances pitch-angle scattering of charged particles.

Figure 1c shows that the average wavenumber at post-saturation does not change much with time in either simulation. For comparison, the values of $k_{\|}$ as computed from linear theory at five times during the simulations are shown as open circles and solid circles for the one- and two-dimensional simulations, respectively. Agreement between theory and simulations is fair for the times shown; the issue of wave energy transfer to longer wavelengths at late times [e.g., *Quest and Shapiro*, 1996] requires computations with larger wave amplitudes and longer times than are used here.

An important difference between our work and earlier computational studies of the firehose [e.g., *Quest and Shapiro*, 1996] is that we have carried out a large number of simulations and have considered our results as a statistical data set from which we induce general conclusions. *McCloskey* [1995] has pointed out that this computational, inductive approach, following the style of ancient Babylonian science, is less elegant that the analytic, deductive approach favored by early Greek scientists. Nevertheless, the continually decreasing cost of computation implies that the Babylonian approach now can compete successfully with the Grecian tradition in plasma physics theory. We believe our recent results, including those described here, concerning proton temperature anisotropy bounds represent an effective use of both traditions in cooperation.

2. Linear Theory

The results of this section are obtained from the linear Vlasov dispersion equation for electromagnetic instabilities in a homogeneous plasma which are driven by a bi-Maxwellian proton distribution. We assume that the electrons (subscript e), as well as the protons, may be represented by bi-Maxwellian velocity distributions, that there is no relative drift between the electrons and protons, and that charge neutrality $n_e = n_p$ holds.

Under the condition $T_{\|p} > T_{\perp p}$ the proton firehose instability may arise as a right-hand circularly polarized mode at $\mathbf{k} \times \mathbf{B}_o = 0$. The firehose has maximum growth rate at $\theta = 0^o$ [*Gary et al.*, 1976], with the angular range of fast growth increasing with $\beta_{\|p}$. For example, for $\gamma_m/\Omega_p = 0.10$, $\gamma(\theta)$ drops to one-half its field-aligned value at $\theta = 22^o$ if $\beta_{\|p} = 2.0$ and at $\theta = 37^o$ if $\beta_{\|p} = 100$. To derive the linear theory threshold expressions, we consider only the condition of maximum growth rate, corresponding to $\mathbf{k} \times \mathbf{B}_o = 0$, in which case the linear dispersion equation is equation (7.1.6) of *Gary* [1993].

A solution to this dispersion equation for a particular mode is determined if the following dimensionless parameters are specified: v_A/c, $T_{\perp p}/T_{\|p}$, $T_{\|e}/T_{\|p}$, $T_{\perp e}/T_{\|e}$, and the parallel β of one species. If $v_A/c << 1$, the firehose is essentially independent of this parameter, so we choose $v_A/c = 2.4 \times 10^{-4}$. To begin, we choose $T_{\|e}/T_{\|p} = 1$ and, to isolate the consequences of the proton anisotropy, $T_{\perp e}/T_{\|e} = 1$. Then the threshold condition on the proton anisotropy can be expressed solely as a function of $\beta_{\|p}$.

Electrons are nonresonant ($|\zeta_e^+| >> 1$) at the maximum growth rate of this mode, but protons may be either cyclotron resonant or nonresonant, as Figure 2 demonstrates. For relatively strong growth rates ($\gamma_m/\Omega_p \gtrsim 0.05$) the protons are resonant at maximum growth ($1 < |\zeta_p^+| \lesssim 3$) on the domain $1 \lesssim \beta_{\|p} \leq 100$. As γ_m/Ω_p decreases, the firehose remains resonant at $\beta_{\|p} \lesssim 20$, but at larger values

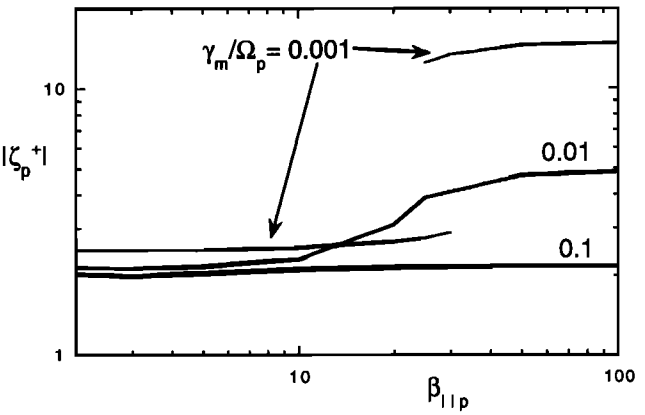

Figure 2. Linear theory results: the proton cyclotron resonance factor at the wavenumber of maximum growth of the proton firehose instability as a function of the parallel proton β for three values of the maximum growth rate.

of this parameter, the maximum growth rate shifts to very small wavenumbers where $|\zeta_p^+| >> 1$ and the instability becomes fluid-like with $|\omega_r| \sim \gamma$.

Representative dispersion relations for the firehose instability may be found in the literature and are not shown here. Dispersion is usually parabolic ($\omega_r \sim k^2$). At strong growth rates and most values of $\beta_{\|p}$, the growth rate is positive over a relatively broad range of wavenumbers which includes arbitrarily small $k_{\|}$ [e.g., *Quest and Shapiro*, 1996, Figure 2]. However, as γ_m/Ω_p decreases, the domain of unstable wavenumbers shrinks and the resonant mode is no longer unstable at arbitrarily long wavelengths [e.g., *Gary*, 1993, Figure 7.2; *Xue et al.*, 1993, Figure 2].

The simulations to be described later use initial conditions at relatively strong growth rates ($\gamma_m/\Omega_p \geq 0.05$), so that, by Figure 2, protons should be uniformly resonant for these computations. Therefore we here outline the derivation of the firehose threshold condition for resonant protons. The procedure is similar to that of *Gary and Lee* [1994] for the threshold of the proton cyclotron anisotropy instability. If the electrons are nonresonant and we assume that $\gamma_m \simeq 0$,

$$\mathrm{Im}[S_p^+(\mathbf{k},\omega)] = 0$$

where S_p^+ is the dimensionless conductivity of the protons for fluctuations of positive helicity [e.g., *Gary*, 1993, Equation (7.1.7)]. Then, by the usual arguments one obtains

$$1 - \frac{T_{\perp p}}{T_{\|p}} = \frac{1}{\zeta_p^+}\left(\frac{\omega_r}{k_{\|}v_A}\right)\left(\frac{1}{\beta_{\|p}}\right)^{0.50} \qquad (5)$$

For $1 \leq \beta_{\|p} \leq 10$, least-squares fits to firehose solutions of the dispersion equation yield

$$\frac{\omega_r}{k_{\|}v_A} \simeq \frac{1.40}{\beta_{\|p}^{0.16}} \quad \text{at} \quad \gamma_m = 10^{-3}\Omega_p,$$

$$\frac{\omega_r}{k_{\|}v_A} \simeq \frac{1.46}{\beta_{\|p}^{0.21}} \quad \text{at} \quad \gamma_m = 10^{-2}\Omega_p,$$

$$\frac{\omega_r}{k_{\|}v_A} \simeq \frac{1.05}{\beta_{\|p}^{0.13}} \quad \text{at} \quad \gamma_m = 10^{-1}\Omega_p.$$

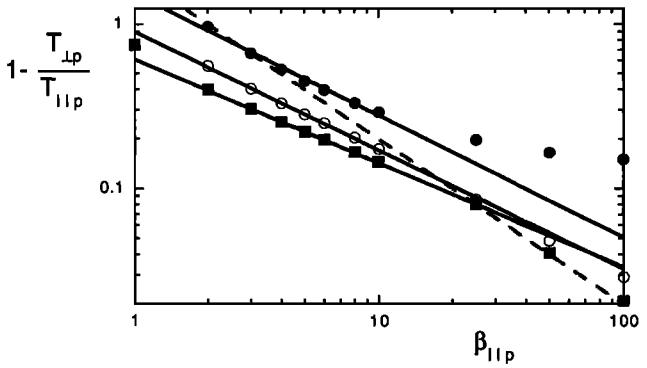

Figure 3. Linear theory results: the proton temperature anisotropy as a function of $\beta_{\|p}$ for the proton firehose instability under the threshold conditions $\gamma_m/\Omega_p = 0.001$ (solid squares), 0.01 (open circles), and 0.1 (solid circles). The three solid lines represent the three results of (6), and the dashed line indicates (1), the instability condition of the nonresonant proton firehose.

From Figure 2 for $1 \leq \beta_{\|p} \leq 10$,

$$\mathrm{Re}(\zeta_p^+) \simeq 2.5 \text{ at } \gamma_m = 10^{-3}\Omega_p,$$

$$\mathrm{Re}(\zeta_p^+) \simeq 2.2 \text{ at } \gamma_m = 10^{-2}\Omega_p,$$

$$\mathrm{Re}(\zeta_p^+) \simeq 2.0 \text{ at } \gamma_m = 10^{-1}\Omega_p.$$

Therefore (5) is of the form of (2) with

$$S_p = 0.56 \text{ and } \alpha_p = 0.66 \text{ at } \gamma_m = 10^{-3}\Omega_p,$$

$$S_p = 0.66 \text{ and } \alpha_p = 0.71 \text{ at } \gamma_m = 10^{-2}\Omega_p,$$

$$S_p = 0.53 \text{ and } \alpha_p = 0.63 \text{ at } \gamma_m = 10^{-1}\Omega_p.$$

By applying the least-squares fitting procedure directly to firehose solutions of the dispersion equation on the domain $2 \leq \beta_{\|p} \leq 10$ we obtain similar results at $\gamma_m/\Omega_p \leq 10^{-2}$:

$$S_p = 0.61 \text{ and } \alpha_p = 0.63 \text{ at } \gamma_m = 10^{-3}\Omega_p, \quad (6a)$$

$$S_p = 0.90 \text{ and } \alpha_p = 0.72 \text{ at } \gamma_m = 10^{-2}\Omega_p, \quad (6b)$$

$$S_p = 1.53 \text{ and } \alpha_p = 0.74 \text{ at } \gamma_m = 10^{-1}\Omega_p. \quad (6c)$$

Figure 3 illustrates individual computed linear theory results as well as the least-squares fits to (2) with parameters as given by (6). The fits to the two lower growth rates provide a good approximation over the domain $1 \leq \beta_{\|p} \leq 25$. At $\beta_{\|p} \gtrsim 25$ and $\gamma_m/\Omega_p < 0.01$ the firehose becomes nonresonant. This effect appears in Figure 3 as high-β increases in the slopes of the plots corresponding to $\gamma_m/\Omega_p = 0.01$ and 10^{-3}. In particular the latter case approaches the well-known fluid theory threshold condition $1 - T_{\perp p}/T_{\|p} = 2/\beta_{\|p}$ [*Parker*, 1958].

Electrons have a nonresonant cyclotron interaction with the firehose, so we expect that these threshold conditions are essentially independent of the electron/proton temperature ratio, and sample computations confirm this over the domains $2 \leq \beta_{\|p} \leq 100$ and $0.10 \leq T_{\|e}/T_{\|p} \leq 10.0$. However, even though $|\zeta_e^+| >> 1$, electron anisotropies lead to nontrivial frequency shifts for the proton firehose instability and thereby significantly affect both growth rates and thresholds for this growing mode [*Kennel and Scarf*, 1968; *Hollweg and Völk*, 1970]. $T_{\perp e} > T_{\|e}$ reduces the firehose growth rate and thereby raises the proton anisotropy at threshold, whereas $T_{\perp e} < T_{\|e}$ has the opposite effect. The hybrid simulations described in the following two sections utilize an isotropic fluid electron model, so the linear theory results developed in this section should be applicable to our computations. However, any comparison of our results against observations will require a knowledge of and, if necessary, a compensation for any electron anisotropy which may be present.

3. One-Dimensional Simulations

This section describes results from one-dimensional hybrid simulations [*Winske and Omidi*, 1993] in which the plasma is initially spatially homogeneous and periodic boundary conditions are imposed. At $t = 0$ the proton velocity distribution is bi-Maxwellian with $T_{\|p} > T_{\perp p}$ and $T_e = T_{\|p}$. Here θ, the angle between $\mathbf{B}_o$ and the orientation of the simulation, is chosen as 0^o for all our runs. The simulations are carried out in a system with 128 cells, a system length $L\omega_p/c$ approximately equal to four times the wavelength of the fastest growing mode, 400 superparticles per cell, and an integration time step of $\Omega_p \Delta t = 0.05$. Table 1 gives the initial conditions for each simulation in our ensemble; we consider $0.05 \leq \gamma_m/\Omega_p \leq 0.30$ and $2.0 \leq \beta_{\|p} \leq 100$. Figure 2 demonstrates that these parameters correspond to resonant wave-proton interactions. Furthermore, the finite length of the system excludes the longest

Table 1. Initial Conditions for Simulations and Corresponding Linear Theory Results

$\beta_{\|p}$	$T_{\perp p}/T_{\|p}$	$L\omega_p/c$	γ_m/Ω_p	$k_m c/\omega_p$
2.00	0.20	42.0	0.05	0.60
5.00	0.64	95.0	0.05	0.27
10.00	0.78	166.0	0.05	0.15
25.00	0.88	299.0	0.05	0.08
50.00	0.91	441.0	0.05	0.06
100.0	0.93	628.0	0.05	0.04
2.00	0.03	48.0	0.10	0.53
5.00	0.55	94.0	0.10	0.27
10.00	0.71	147.0	0.10	0.17
25.00	0.80	246.0	0.10	0.10
50.00	0.83	349.0	0.10	0.07
100.0	0.85	502.0	0.10	0.05
5.00	0.31	74.0	0.20	0.34
10.00	0.48	108.0	0.20	0.23
25.00	0.58	175.0	0.20	0.14
50.00	0.62	246.0	0.20	0.10
100.0	0.63	347.0	0.20	0.07
5.00	0.01	56.0	0.30	0.45
10.00	0.20	79.0	0.30	0.32
25.00	0.32	125.0	0.30	0.20
50.00	0.35	177.0	0.30	0.14
100.0	0.37	249.0	0.30	0.10

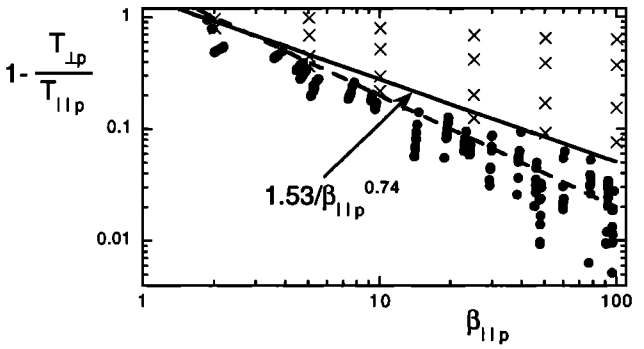

Figure 4. Results from one-dimensional hybrid simulations at $\theta = 0^o$ under the initial conditions described in Table 1. Here the proton temperature anisotropies are plotted as functions of the corresponding $\beta_{\|p}$ values. Parameters at $t = 0$ are represented by crosses, and parameters at post-saturation times ($\Omega_p t = 50, 100, 150, \ldots 400$) are represented by solid circles. The solid line represents (2) with $S_p = 1.53$ and $\alpha_p = 0.74$, whereas the dashed line represents (1), the instability condition of the nonresonant proton firehose.

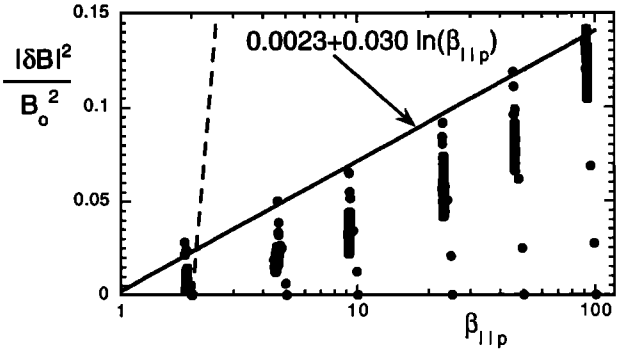

Figure 5. Results from one-dimensional hybrid simulations at $\theta = 0^o$ under the initial conditions described in Table 1 and $\gamma_m/\Omega_p = 0.10$. Here the fluctuating field energy densities at $\Omega_p t = 10, 20, 30, \ldots 400$ are plotted as solid circles. The solid curve represents an approximate bounding curve of the form of (3) with $S_B = 0.0023$ and $\alpha_p = 0.030$, and the dashed line represents (4).

wavelength nonresonant modes, so that our simulations address the resonant case almost exclusively.

Quest and Shapiro [1996] reported results from three one-dimensional hybrid simulations of the proton firehose instability under the initial condition $T_{\perp p} = 0$. After saturation they found a second stage of slower evolution during which the fluctuating field energy spectrum exhibits a cascade to longer wavelengths and the proton anisotropy reduction continues, although at a much slower rate. Our simulations show the same characteristics with the exception of the fluctuation cascade (See Figure 1). Study of this latter issue requires computations with larger amplitude fluctuations and/or longer times than those used here.

In contrast to *Quest and Shapiro* [1996], we have executed a relatively large number of firehose simulations with a variety of initial values of $T_{\perp p}/T_{\|p}$. The one-dimensional results shown in Figure 1 are characteristic of these runs; the growth of magnetic fluctuations leads to wave-particle scattering which reduces $T_{\|p}$ and increases $T_{\perp p}$ so that both the anisotropy and $\beta_{\|p}$ are reduced. The simulation results for anisotropies over $0 \leq \Omega_p t \leq 400$ are summarized in Figure 4; the post-saturation anisotropies uniformly lie on or below a line given by (2) with $S_p = 1.53$ and $\alpha_p = 0.74$. This condition is shown as the solid line in Figure 4 and corresponds to the linear Vlasov threshold condition for growth of the firehose instability at $\gamma_m/\Omega_p = 0.10$ over $2.0 \leq \beta_{\|p} \leq 10$. For this ensemble of simulations the threshold condition derived from fluid theory [the dashed line in Figure 4 corresponding to (1)] provides an inferior constraint for the post-saturation anisotropies.

It is not useful to associate simulation results with (1) or (2) unless the proton distribution remains approximately bi-Maxwellian. Our one- and two-dimensional simulations of the proton cyclotron instability [*Gary et al.*, 1996; 1997] showed that enhanced fluctuations from this mode preserve the initially bi-Maxwellian character of a proton distribution for a broad range of parameters. Here we used the one-dimensional hybrid code to examine the same question for enhanced firehose fluctuations. Sampling several of the runs listed in Table 1, we found that, indeed, the proton distributions remained approximately bi-Maxwellian.

If one considers an ensemble of simulations with a broad range of initial growth rates, as we have done here, the post-saturation temperature anisotropy bound is independent of the initial γ_m/Ω_p. However, the maximum value of the fluctuating field energy is not independent of the initial growth; for a fixed $\beta_{\|p}$ a larger initial anisotropy leads to a larger field amplitude at saturation. Therefore we seek an upper bound to $|\delta B|^2/B_o^2$ as a function of both $\beta_{\|p}$ and γ_m/Ω_p. A representative result from our simulations with initial $\gamma_m/\Omega_p = 0.10$ is shown in Figure 5; this result, as for each of the four initial growth rates described in Table 1, is approximately bounded by the form of (3). The parameters of the approximate bounding curves which we have obtained from the runs of Table 1 are stated in Table 2.

Our simulations, as well as those of *Quest and Shapiro* [1996], yield field amplitudes at large $\beta_{\|p}$ which are considerably weaker than the nonresonant prediction of (4). This is illustrated in Figure 5, where the dashed line representing (4) does not provide a useful constraint on our simulation results for the initial value $\gamma_m/\Omega_p = 0.10$. This difference is clearly due to the resonant character of the instability simulated here, which corresponds to a stronger wave-particle interaction and implies a lower saturation amplitude than the fluid theory prediction.

4. Two-Dimensional Simulations

This section describes results from two-dimensional hybrid simulations [*Winske and Omidi*, 1993] in which the

Table 2. Empirical Parameters for Fluctuating Magnetic Fields Constrained by (3)

γ_m/Ω_p	S_B (1-D)	α_B (1-D)	S_B (2-D)	α_B (2-D)
0.05	−0.013	0.020	−0.004	0.010
0.10	0.0023	0.030	0.012	0.015
0.20	0.043	0.084	0.13	0.037
0.30	0.42	0.15	0.46	0.065

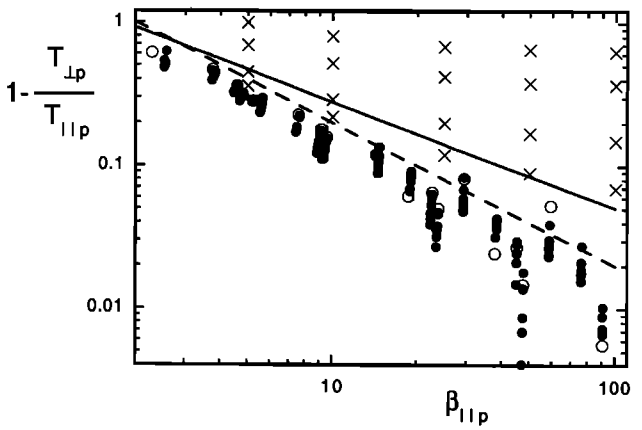

Figure 6. Results from two-dimensional hybrid simulations under the initial conditions described in Table 1 for $\beta_{\|p} \geq 5.0$. Here the proton temperature anisotropies are plotted as functions of the corresponding $\beta_{\|p}$ values. Parameters at $t = 0$ are represented by crosses, those at saturation are represented by open circles, and those at successive post-saturation intervals of $\Delta\Omega_p t = 25$ are represented by solid circles. The solid line represents (2) with $S_p = 1.53$ and $\alpha_p = 0.74$ whereas the dashed line represents the nonresonant firehose instability condition (1).

plasma is initially spatially homogeneous and there is a single initially bi-Maxwellian proton velocity distribution with $T_{\|p} > T_{\perp p}$. The electrons are represented as a massless fluid with $T_e = T_{\|p}$ at $t = 0$. We use a doubly periodic system in x and y with the background magnetic field $\mathbf{B}_o = \hat{\mathbf{x}} B_o$. We have used a 64 × 64 grid, system dimensions $L_x = L_y = L$ with $L\omega_p/c$ approximately equal to four times the wavelength of the proton anisotropy mode with largest growth rate, an integration time step of $\Omega_p \Delta t = 0.10$, and a small resistivity to reduce short wavelength fluctuations.

The number of superparticles per cell N is a critical parameter in these simulations. Early two-dimensional simulation studies of the proton cyclotron instability [*Thomas and Brecht*, 1986; *Winske and Quest*, 1988] used $10 \lesssim N \lesssim 20$, a number adequate for yielding qualitative results for relatively large initial growth rates ($\gamma_m \gtrsim \Omega_p$). As computing power and speed have increased, it has become practical to use substantially larger numbers of particles per cell (e.g., $N \simeq 144$ by *McKean et al.* [1994]), enabling us to carry out a quantitative study of firehose properties at relatively modest initial growth rates ($\gamma_m \simeq 0.1\Omega_p$). After several test runs we determined that appropriate results can be obtained from runs with 256 superparticles per cell.

Using these parameters, we repeated the ensemble of simulations described in Table 1, excluding the two runs starting with $\beta_{\|p} = 2.0$. As with the one-dimensional simulations, the fluctuating fields grew rapidly to saturation as the temperature anisotropy was reduced; after saturation the field amplitude and proton anisotropy both typically showed gradual decreases (e.g., as in Figure 1).

Temperature anisotropies for this ensemble of two-dimensional runs are summarized in Figure 6. As in the specific case of Figure 1, the fluctuating field saturation amplitudes and late time anisotropies are generally smaller in the two-dimensional simulations than in the one-dimensional runs. Although under the same initial conditions two-dimensional simulations typically yield somewhat smaller values of $|\delta B|^2/B_o^2$, the broader spectrum of two-dimensional fluctuations appears to be more efficient at scattering the protons, yielding a smaller proton anisotropy. The best upper bound for post-saturation temperature anisotropies is not provided by (2) with a resonant condition $\alpha_p \simeq 0.7$ but rather by the nonresonant stability criterion (1), as indicated by the dashed line in Figure 6. As we noted in section 2, at $\beta_{\|p} \geq 25$ the firehose becomes nonresonant for small growth rates, so that at such high values of the parallel proton β a fluid-like response might be expected. At smaller values of $\beta_{\|p}$ the difference between the predictions of fluid and kinetic theory becomes relatively small, and it is difficult to discern which is the more appropriate constraint.

The two-dimensional results for the maximum value of the fluctuating magnetic field energy as a function of $\beta_{\|p}$ are qualitatively similar to the one-dimensional results of Figure 5. The maximum values for a fixed initial value of γ_m/Ω_p scale as (3), and the empirical parameters are as given in Table 2. As indicated by Figure 1 and as is the case for electromagnetic instabilities driven by $T_{\perp p} > T_{\|p}$ [*Gary et al.*, 1997], the maximum fluctuating magnetic field energies from the firehose at $\beta_{\|p} >> 1$ are somewhat larger for the one-dimensional simulations than for comparable conditions in the two-dimensional runs. Results for runs with initial values $\gamma_m/\Omega_p = 0.10$ are illustrated in Figure 7. Here, as with all choices of the initial growth rate, the empirical scaling of (3) provides a much better constraint on the fluctuating fields than the fluid-theoretical equation (4).

5. Conclusions

We used linear Vlasov dispersion theory in a homogeneous plasma to show that (2) with $\alpha_p \simeq 0.7$ represents the threshold condition for the proton resonant firehose instability over $1 \lesssim \beta_{\|p} \lesssim 25$. We then carried out one- and two-dimensional hybrid simulations with maximum initial growth rates $\gamma_m \geq 0.05\ \Omega_p$ on the domain $2 \leq \beta_{\|p} \leq 100$. Under these conditions, enhanced fluctuations from the firehose correspond to predominantly resonant wave-proton interactions, and our one-dimensional runs yield a

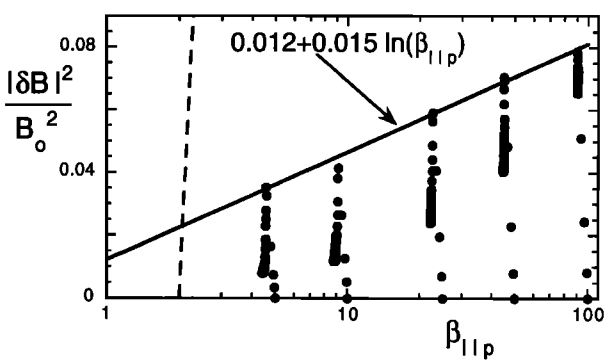

Figure 7. Results from two-dimensional hybrid simulations under the initial conditions described in Table 1 for $\beta_{\|p} \geq 5.0$ and $\gamma_m/\Omega_p = 0.10$. Here the fluctuating field energy densities at $\Omega_p t = 10, 20, 30, \ldots 200$ are plotted as solid circles. The solid curve represents an approximate bounding curve of the form of (3) with $S_B = 0.012$ and $\alpha_p = 0.015$, and the dashed line represents (4).

proton temperature anisotropy upper bound which is commensurate with a resonant threshold condition. However, the presumably more realistic two-dimensional simulations yield a post-saturation upper bound on the proton temperature anisotropy which approximately corresponds to the nonresonant fluid stability condition (1). Although the difference between the nonresonant and resonant criteria is small, the result that a predominantly resonant instability should lead to a nonresonant anisotropy bound is both surprising and deserving of further study. Our simulations also demonstrated that the field energy density of these fluctuations is bounded by the form of (3) on this same domain, an apparently resonant result which is clearly distinguishable from the nonresonant theory prediction of (4).

The nonresonant proton anisotropy bound corresponding to (1) has already been used as a bound in the anisotropic MHD models of *Nötzel et al.* [1985] and *Cao and Lee* [1994]. We recommend the use of this constraint in any anisotropic MHD model with $\beta_{\|p} > 1$.

The primary limiting assumption here is that the protons are well represented as a single bi-Maxwellian velocity distribution. In situ observations of space plasmas often show that, even if $T_{\|p} > T_{\perp p}$ in an average sense, the apparently large parallel temperature is due to the relative streaming of two distinguishable components [e.g., *Marsch*, 1991]. The linear properties of instabilities driven by such distributions are quite different from those of the firehose [e.g., *Gary*, 1993, chap. 8]; in particular, electromagnetic ion/ion instabilities may grow at $\beta_{\|p} << 1$. Thus the results obtained here should be applied only to plasmas in which the proton distribution is observed to be approximately bi-Maxwellian. Given this condition, we predict that both (1) and (3) should be observable as upper bounds on their respective quantities in any sufficiently homogeneous space plasma. The fluid form of the anisotropy bound, (1), should be appropriate, but we predict that our form of the fluctuating field energy bound, (3), obtained from proton cyclotron resonant simulations, should be observed, rather than the nonresonant prediction of (4). Analysis of solar wind particle and fluctuation data should clearly demonstrate which expression is more appropriate.

Appendix

Our notation follows that of *Gary* [1993]; in particular, the cyclotron resonance factor for the jth species is $\zeta_j^{\pm} \equiv (\omega \pm \Omega_j)/\sqrt{2}|k_{\|}|v_j$, where the thermal speed of the jth component is $v_j = \sqrt{k_B T_{\|j}/m_j}$, the cyclotron frequency of the j species is $\Omega_j = e_j B_o/m_j c$, and the complex frequency is $\omega = \omega_r + i\gamma$. Here $\beta_{\|p} \equiv 8\pi n_p T_{\|p}/B_o^2$. We assume throughout that the protons (denoted by subscript p) may be represented by a single bi-Maxwellian zeroth-order velocity distribution and that heavy ion species may be ignored. The maximum growth rate from linear theory for a given set of dimensionless parameters is denoted by γ_m, the angle between $\mathbf{k}$ and $\mathbf{B}_o$ is θ, and the Alfvén speed is $v_A \equiv \sqrt{B_o^2/4\pi n_p m_p}$.

Acknowledgments. We acknowledge useful discussions with Bill Daughton. This work was performed under the auspices of the U.S. Department of Energy (DOE) and was supported by the DOE Office of Basic Energy Sciences, Division of Engineering and Geosciences, the Space Plasma Theory Program of the National Aeronautics and Space Administration (NASA), and the Laboratory Directed Research and Development Program at Los Alamos.

The Editor thanks H. Karimabadi and another referee for their assistance in evaluating this paper.

References

Anderson, B. J., S. A. Fuselier, S. P. Gary, and R. E. Denton, Magnetic spectral signatures in the Earth's magnetosheath and plasma depletion layer, *J. Geophys. Res.*, *99*, 5877, 1994.

Anderson, B. J., R. E. Denton, G. Ho, D. C. Hamilton, S. A. Fuselier, and R. J. Strangeway, Observational test of local proton cyclotron instability in the Earth's magnetosphere, *J. Geophys. Res.*, *101*, 21,527, 1996.

Birn, J., S. P. Gary, and M. Hesse, Microscale anisotropy reduction and macroscale dynamics of the magnetotail, *J. Geophys. Res.*, *100*, 19,211, 1995.

Cao, F., and L. C. Lee, Plasma pressure and anisotropy inferred from the Tsyganenko magnetic field model, *Ann. Geophys.*, *12*, 286, 1994.

Denton, R. E., and J. G. Lyon, Density depletion in an anisotropic magnetosheath, *Geophys. Res. Lett.*, *23*, 2891, 1996.

Fuselier, S. A., B. J. Anderson, S. P. Gary, and R. E. Denton, Inverse correlations between the ion temperature anisotropy and plasma beta in the Earth's quasi-parallel magnetosheath, *J. Geophys. Res.*, *99*, 14,931, 1994.

Gary, S. P., *Theory of Space Plasma Microinstabilities*, Cambridge Univ. Press, New York, 1993.

Gary, S. P., and M. A. Lee, The ion cyclotron anisotropy instability and the inverse correlation between proton anisotropy and proton beta, *J. Geophys. Res.*, *99*, 11,297, 1994.

Gary, S. P., M. D. Montgomery, W. C. Feldman, and D. W. Forslund, Proton temperature anisotropy instabilities in the solar wind, *J. Geophys. Res.*, *81*, 1241, 1976.

Gary, S. P., M. F. Thomsen, L. Yin, and D. Winske, Electromagnetic proton cyclotron instability: Interactions with magnetospheric protons, *J. Geophys. Res.*, *100*, 21,961, 1995.

Gary, S. P., V. M. Vazquez, and D. Winske, Electromagnetic proton cyclotron instability: Proton velocity distributions, *J. Geophys. Res.*, *101*, 13,327, 1996.

Gary, S. P., J. Wang, D. Winske, and S. A. Fuselier, Proton temperature anisotropy upper bound, *J. Geophys. Res.*, *102*, 27,159, 1997.

Hollweg, J. V., and H. J. Völk, New plasma instabilities in the solar wind, *J. Geophys. Res.*, *75*, 5297, 1970.

Karimabadi, H., D. Krauss-Varban, and T. Terasawa, Physics of pitch angle scattering and velocity diffusion, 1. Theory, *J. Geophys. Res.*, *97*, 13,853, 1992.

Kennel, C. F., and H. E. Petschek, Limit on stably trapped particle fluxes, *J. Geophys. Res.*, *71*, 1, 1966.

Kennel, C. F., and F. L. Scarf, Thermal anisotropies and electromagnetic instabilities in the solar wind, *J. Geophys. Res.*, *73*, 6149, 1968.

Manheimer, W., and J. P. Boris, Marginal stability analysis–A simpler approach to anomalous transport in plasmas, *Comments Plasma Phys. Controlled Fusion*, *3*, 15, 1977.

Marsch, E., Kinetic physics of the solar wind plasma, in *Physics of the Inner Heliosphere II*, edited by R. Schwenn and E. Marsch, p. 45, Springer-Verlag, New York, 1991.

McCloskey, D. N., Computation outstrips analysis, *Sci. Am.*, *273*, 26, 1995.

McKean, M. E., D. Winske, and S. P. Gary, Two-dimensional simulations of ion anisotropy instabilities in the magnetosheath, *J. Geophys. Res.*, *99*, 11,141, 1994.

Nötzel, A., K. Schindler, and J. Birn, On the cause of approximate pressure isotropy in the quiet near-Earth plasma sheet, *J. Geophys. Res.*, *90*, 8293, 1985.

Parker, E. N., Dynamical instability in an anisotropic ionized gas of low density, *Phys. Rev.*, *109*, 1874, 1958.

Quest, K. B., and V. D. Shapiro, Evolution of the fire-hose instability: Linear theory and wave-wave coupling, *J. Geophys. Res.*, *101*, 24,457, 1996.

Thomas, V. A., and S. H. Brecht, Two-dimensional simulation of high Mach number plasma interactions, *Phys. Fluids*, *29*, 2444, 1986.

Vedenov, A. A., and R. Z. Sagdeev, Some properties of the plasma with anisotropic distribution of the velocities of ions in the magnetic field, *Dokl. Akad. Nauk. SSSR*, *3*, 278, 1958.

Winske, D., and N. Omidi, Hybrid codes: Methods and applications, in *Computer Space Plasma Physics: Simulation Techniques and Software*, edited by H. Matsumoto and Y. Omura, p. 103, Terra Sci., Tokyo, 1993.

Winske, D., and K. B. Quest, Magnetic field and density fluctuations at perpendicular supercritical collisionless shocks, *J. Geophys. Res.*, *93*, 9681, 1988.

Xue, S., R. M. Thorne, and D. Summers, Electromagnetic ion-cyclotron instability in space plasmas, *J. Geophys. Res.*, *98*, 17,475, 1993.

Yoon, P. H., Electromagnetic fire-hose instability in a fully relativistic bi-Maxwellian plasma, *Phys. Fluids B*, *2*, 842, 1990.

S. P. Gary, Los Alamos National Laboratory, M.S. D466, Los Alamos, NM 87545. (e-mail: pgary@lanl.gov; URL: http://nis-www.lanl.gov/~pgary/).

H. Li, Los Alamos National Laboratory, M.S. D436, Los Alamos, NM 87545. (e-mail: hli@lanl.gov).

S. O'Rourke, Los Alamos National Laboratory, M.S. D466, Los Alamos, NM 87545. (e-mail: seano@nis.lanl.gov).

D. Winske, Los Alamos National Laboratory, M.S. B259, Los Alamos, NM 87545. (e-mail: winske@lanl.gov).

(Received November 11, 1997; revised February 27, 1998; accepted March 30, 1998.)